Spectroscopic intravascular photoacoustic imaging of lipids in atherosclerosis

Krista Jansen
Antonius FW van der Steen
Min Wu
Heleen MM van Beusekom
Geert Springeling
Xiang Li
Qifa Zhou
K. Kirk Shung
Dominique PV de Kleijn
Gijs van Soest

Spectroscopic intravascular photoacoustic imaging of lipids in atherosclerosis

Krista Jansen,[a,b] Antonius FW van der Steen,[a,b,c] Min Wu,[a] Heleen MM van Beusekom,[a] Geert Springeling,[d] Xiang Li,[e] Qifa Zhou,[e] K. Kirk Shung,[e] Dominique PV de Kleijn,[b,f,g] and Gijs van Soest[a,*]
[a]Unit Experimental Cardiology, Thorax Center, Department of Biomedical Engineering, Erasmus MC, Rotterdam, PO Box 2040, 3000 CA Rotterdam, The Netherlands
[b]Interuniversity Cardiology Institute of The Netherlands—Netherlands Heart Institute, PO Box 19258, 3501 DG, Utrecht, The Netherlands
[c]Delft University of Technology, Department of Imaging Science and Technology, Lorentzweg 1, 2628 CJ Delft, The Netherlands
[d]Experimental Medical Instruments, Department of Experimental Medical Instruments, Erasmus MC, PO Box 2040, 3000 CA Rotterdam, The Netherlands
[e]University of Southern California, Department of Biomedical Engineering, Los Angeles, California 90089
[f]Cardiovascular Research Institute, National University Heart Center, 5 Lower Kent Ridge Road Singapore 119074, Singapore
[g]University Medical Center Utrecht, Laboratory of Experimental Cardiology, Heidelberglaan 100 3584 CX Utrecht, The Netherlands

Abstract. The natural history of atherosclerosis is marked by changes in the lipid biochemistry in the diseased arterial wall. As lesions become more vulnerable, different cholesterol species accumulate in the plaque. Understanding unstable atherosclerosis as a pharmacological and interventional therapeutic target requires chemically specific imaging of disease foci. In this study, we aim to image atherosclerotic plaque lipids and other vessel wall constituents with spectroscopic intravascular photoacoustics (sIVPA). sIVPA imaging can identify lipids in human coronary atherosclerotic plaque by relying on contrast in the near-infrared absorption spectra of the arterial wall components. Using reference spectra acquired on pure compounds, we analyzed sIVPA data from human coronary plaques *ex vivo*, to image plaque composition in terms of cholesterol and cholesterol ester content. In addition, we visualized the deeper lying connective tissue layers of the adventitia, as well as the fatty acid containing adipose cells in the peri-adventitial tissue. We performed simultaneous coregistered IVUS imaging to obtain complementary morphological information. Results were corroborated by histopathology. sIVPA imaging can distinguish the most prevalent lipid components of human atherosclerotic plaques and also visualize the connective tissue layers of the adventitia and the fatty acid containing adipose cells in the peri-adventitial tissue. © *2014 Society of Photo-Optical Instrumentation Engineers (SPIE)* [DOI: 10.1117/1.JBO.19.2.026006]

1 Introduction

Atherosclerosis is a chronic cardiovascular disease characterized by inflammation and lipid accumulation in the vessel wall. Myocardial infarctions are a leading cause of death worldwide.[1] In the majority of cases, myocardial infarctions and strokes are caused by the rupture of an atherosclerotic plaque and the subsequent release of its thrombogenic content into the bloodstream.[2] The term "vulnerable plaque" has been coined to indicate a plaque at high risk of rupture that could lead to thrombosis.[3] The susceptibility of a plaque to rupture, its vulnerability, is known to be related to plaque composition, mechanical stress distribution, inflammatory state,[3,4] and presence of positive remodeling.[5] A prominent type of vulnerable plaque is the thin-cap fibroatheroma. These lesions are characterized by a lipid-rich necrotic core covered by a thin fibrous cap that is weakened by macrophage infiltration and decreased smooth muscle cell content.[6]

The chemical composition of the lipid core is related to the age and stability of a lesion. Starting as a foam cell rich lesion (fatty streak) that contains cholesterol esters, supersaturation leads to cholesterol crystallization and cell death resulting in a more complex atherosclerotic plaque containing a necrotic core.[7]

The necrotic core contains cholesterol crystals and extracellular droplets of cholesterol esters. At the periphery of the lesion, cholesterol esters in foam cells dominate.[8] The esterified lipid concentrations at the edge of advanced plaques often coincide with an increased macrophage activity and decreased cap thickness, leading to a predisposition to rupture.[8] A concurring degradation of the supporting structure in the necrotic core enables its thrombogenic content to freely flow into the bloodstream upon rupture of the cap.[7]

During plaque regression, for instance due to cholesterol lowering drugs or lifestyle changes, cholesterol ester content and numbers of foam cells and macrophages decrease. The lipid content of the cells is deposited in cholesterol crystals and the relative proportion of free cholesterol increases. Prolonged regression returns the lipid content of the artery wall toward normal, slowly dissipating the cholesterol crystals, and results in a lipid-poor but scarred intima.[9] Interestingly, the cholesterol ester spectrum differs between developing and regressing lesions.[7]

Established techniques are unable to positively identify and quantify lipid content, or to distinguish between lipid types present in atherosclerotic plaques. Catheter-based near-infrared reflection spectroscopy (NIRS) uses optical absorption to signal

*Address all correspondence to: Gijs van Soest, E-mail: g.vansoest@erasmusmc.nl

the presence of lipid-core plaque in the coronary wall. It is, however, a sensing technology which cannot locate the position of the lipid-core relative to the lumen boundary.[10] By combining NIRS with intravascular ultrasound (IVUS), the most commonly used intravascular imaging technology in clinics worldwide, morphological information is added but lipid mapping still lacks depth resolution.[11] Other imaging modalities, like IVUS, optical coherence tomography, or X-ray computed tomography, rely on backscatter and signal attenuation to interpret images in terms of tissue type.[12–14] A modality that can assess plaque composition and morphology addresses multiple needs in cardiovascular medicine. It provides a chemical imaging biomarker that may acquire a role in clinical trials of drug or device therapies, to grade and monitor plaque regression. By the same merits, such a technique is a likely candidate to attain a prospective definition of vulnerable plaque, a diagnostic criterion that has been elusive since the concept was proposed.[6,15,16]

Photoacoustic (PA) signals are generated in tissue when the absorption of short laser pulses causes the tissue to thermoelastically expand.[17] Intravascular photoacoustic (IVPA) imaging is a catheter-borne version of PA imaging. It uses the intrinsic contrast in optical absorption between tissue types to visualize different constituents of atherosclerotic plaques. IVPA has been demonstrated to distinguish calcified plaque,[18] atheroma,[19,20] and more specifically lipids[21–23] from healthy vessel wall, as well as the presence of macrophages through the use of exogenous contrast agents.[24] The optical absorption spectrum is chemically specific, which is the basis for distinction of tissue components.

In this article, we first determined the absorption spectra of cholesterol, cholesterol oleate (CE18:1) and linoleate (CE18:2) by PA spectroscopy, to use as reference spectra for lipids present in atherosclerotic lesions, which are primarily enhanced as atherosclerosis progresses.[25] We recently published the first IVPA images of lipids in human coronary atherosclerosis.[21] In the present study, we revisited the data from those experiments and optimized the processing for spectral information content. The reanalysis of the spectroscopic intravascular photoacoustic (sIVPA) data revealed detailed local spectra of the different tissue constituents of the atherosclerotic vessel wall. This analysis demonstrates that sIVPA imaging is capable of differentiating lipid components of atherosclerotic plaques: cholesterol and the two most prominent cholesterol esters, cholesterol oleate, and cholesterol linoleate. In addition, we visualize the deeper lying connective tissue layers of the adventitia, as well as the fatty acid containing adipose cells in the peri-adventitial tissue.

2 Methods

2.1 Integrated Catheter and System for Intravascular Imaging

We designed and built an integrated hybrid IVPA/IVUS catheter, see Fig. 1. Imaging of arteries was performed with the device described in earlier works.[21,26] A functionally similar probe was used for the PA spectroscopy measurements of cholesterol and cholesterol derivates, replacing the first one which broke after the experiment. Light is delivered to the vessel wall through 400-μm-diameter core optical fiber (Pioneer Optics, Bloomfield, Connecticut), and a lead magnesium niobate-lead titanate (PMN-PT) single crystal US transducer (custom built[27]) was used to send and receive US waves. The

tip of the fiber was polished at an angle of 34 deg and covered with a glued-on quartz cap to preserve an air-glass interface deflecting the beam by total reflection. The transducer had a center frequency of 44.5 MHz and a −6-dB fractional bandwidth of 45%. Fiber and transducer were mounted in an assembly with an outer diameter of 1 mm. The fiber tip and transducer center were separated by ∼1.1 mm. The angle between the optical and acoustical beams was 22 deg; the beams overlapped between 0.5 and 4.5 mm from the transducer.

The catheter was connected to a spectroscopy/imaging system.[21] A tunable laser (Vibrant B/355-II, OPOTEK, Santa Clara, California) provided the excitation light (pulse width 5 ns, repetition rate 10 Hz, pulse energy 1.2 mJ at catheter tip) for PA imaging. An arbitrary waveform generator (WW2571A, Tabor Electronics Tel Hanan, Israel) transmitted a Gaussian-modulated cosine wave for pulse echo imaging, which was transmitted to the probe through a custom-built expander and limiter. The received ultrasound and PA signals were band pass filtered (13 to 60 MHz 5th-order Butterworth, custom built), amplified by a 43-dB amplifier (AU1263, Miteq, Hauppauge, New York) and digitized at a sample frequency of 350 MS s^{-1} by a 12-bit data acquisition card (Acqiris DP310, Agilent, Santa Clara, California). A schematic of the experiment and photos of the catheter are shown in Figs. 1(a)–1(c).

2.2 Cadaver Coronary Artery Acquisition and Handling

We obtained coronary arteries from the Department of Pathology of the Erasmus MC at autopsy and imaged them within 24-h post mortem. Consent was obtained from the relatives and the protocol was sanctioned by the Medical Ethics Committee of the Erasmus MC (MEC-2007-081). The specimens were mounted on two cannulas in a tank containing saline solution. Large side branches were closed and arteries were pressurized to 100-mmHg to maintain an open lumen. A photograph of an artery mounted in the setup is shown in Fig. 1(d).

2.3 Combined PA and US Imaging of Human Coronary Arteries

The cadaveric coronary arteries were imaged at room temperature within 24-h post mortem. We performed an IVUS pullback of the arteries (iLab system with Atlantis SR Pro catheters; Boston Scientific, Fremont, California) to find sites of interest, and marked them using suture needles. The combined IVPA/ IVUS catheter was mounted in a rotation/translation stage [Steinmeyer, Albstadt, Germany; see Fig. 1(d)]. The suture needles were located and at these sites coregistered IVPA and IVUS cross-sectional scans were made.

Optical and US transmissions alternate for exactly coregistered data acquisition, as illustrated in Fig. 1(a). This procedure results in IVPA and IVUS images of the arterial cross section, as shown in Figs. 2(a) and 2(b). The acquisition time of one coregistered IVPA/IVUS image is 36 s. The image shown here was acquired at 1210 nm. The IVUS and IVPA data sets may be overlaid to create a compound display [Fig. 2(c)]. Spectral scans were made at selected angles. One scan results in a two-dimensional (2-D) data matrix, shown in Fig. 2(d), containing the PA spectra at the different distances from the catheter. The acquisition time of a 76 wavelengths, 32 times averaged data set is ∼5 min. Local absorption spectra can be extracted,
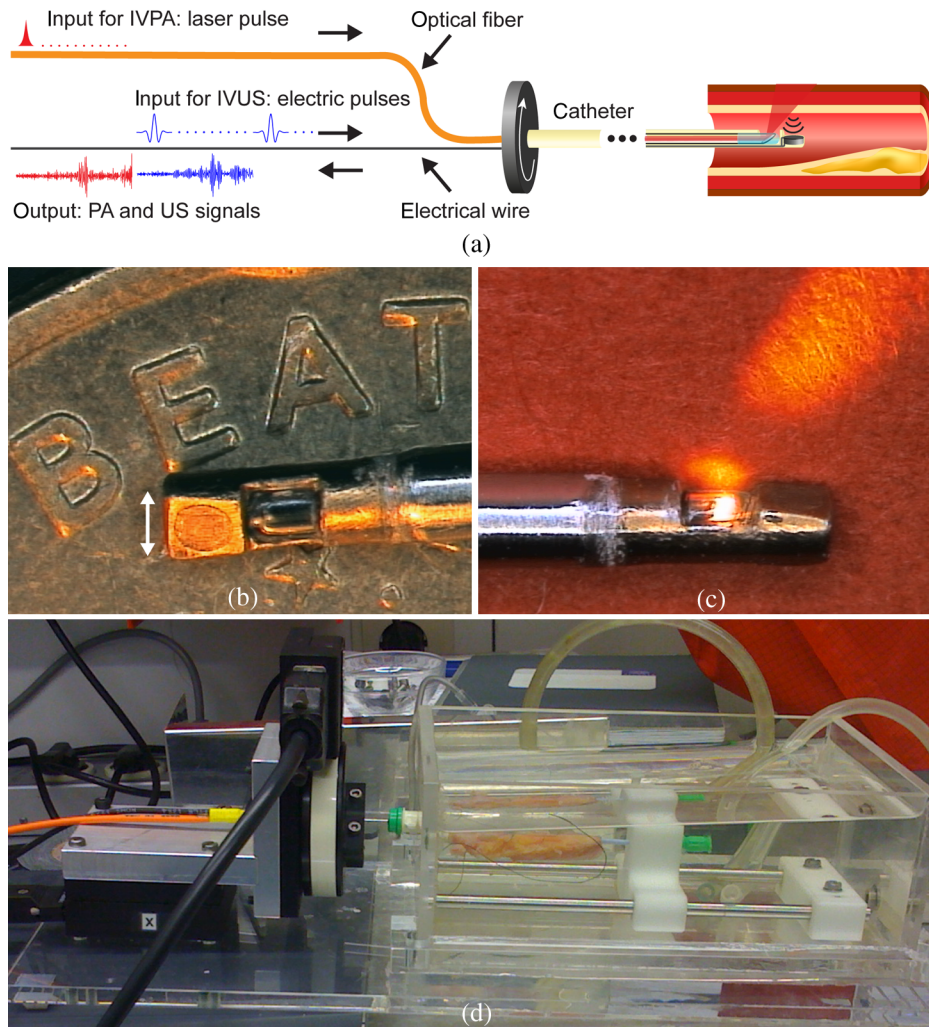
Fig. 1 Combined intravascular photoacoustics (IVPA) and intravascular ultrasound (IVUS) imaging. (a) The intravascular IVPA/IVUS catheter is inserted in an *ex vivo* human coronary artery and rotated in 1 deg steps. Laser pulses for IVPA imaging and electric pulses for pulse echo (IVUS) imaging are delivered to the vessel wall interleaved at every angular position. (b) Photograph of the catheter tip on the edge of a 10 eurocent coin. White arrow indicates 1 mm. (c) Photograph of the catheter tip, showing the light beam exiting the catheter. (d) Photograph of artery in setup, side view. On the left, the translation (*x*) and rotary stage are visible.

as shown in Fig. 2(e). Histology [Oil Red O stain; Fig. 2(f)] confirms the presence of lipids in the areas with a high PA signal at 1210 nm.

US images were created in conventional pulse-echo mode. We transmitted a 10-V peak to peak Gaussian-modulated cosine wave with a center frequency of 30 MHz and a 100% −6-dB bandwidth. 2-D images were obtained by rotating the catheter in 1-deg steps and repeating the US pulse-echo measurement in every direction.

IVPA images were acquired at several excitation wavelengths around 1200 nm. No averaging was applied for IVPA imaging; IVUS traces were averaged 10-fold. Digitized IVPA and IVUS data were band pass filtered (10 to 40 MHz 300th-order zero-phase forward and reverse finite impulse response filter), Tukey windowed, enveloped, and log compressed. The data were then converted to Cartesian coordinates and displayed using the "hot" and "gray" colormaps in MATLAB (The Mathworks, Natick, Massachusetts) for the IVPA and IVUS images, respectively. Combined IVPA/ IVUS images were created by overlaying the IVPA data on IVUS image using a nonlinear red-yellow-white color scale and a linear transparency scale. All data processing was done using MATLAB R2007b.

2.4 PA Spectroscopy of Cholesterol and Cholesterol Derivates

A small volume of lipid material (cholesterol, cholesterol oleate, and cholesterol linoleate; all from Sigma Aldrich Chemie BV, Zwijndrecht, The Netherlands) was mixed with a minimal amount of water to eliminate all air from the sample. The densely packed lipids were then positioned directly in front of the catheter tip. They were contained in a holder, made of TPX (TPX® RT18; Goodfellow, Huntingdon, England) and designed to minimize acoustic reflections. We recorded spectral PA data by recording the signal trace generated by the lipids at wavelengths between 1125 and 1275 nm, spaced by 2 nm. This procedure resulted in a 2-D data set as in Fig. 2(d).
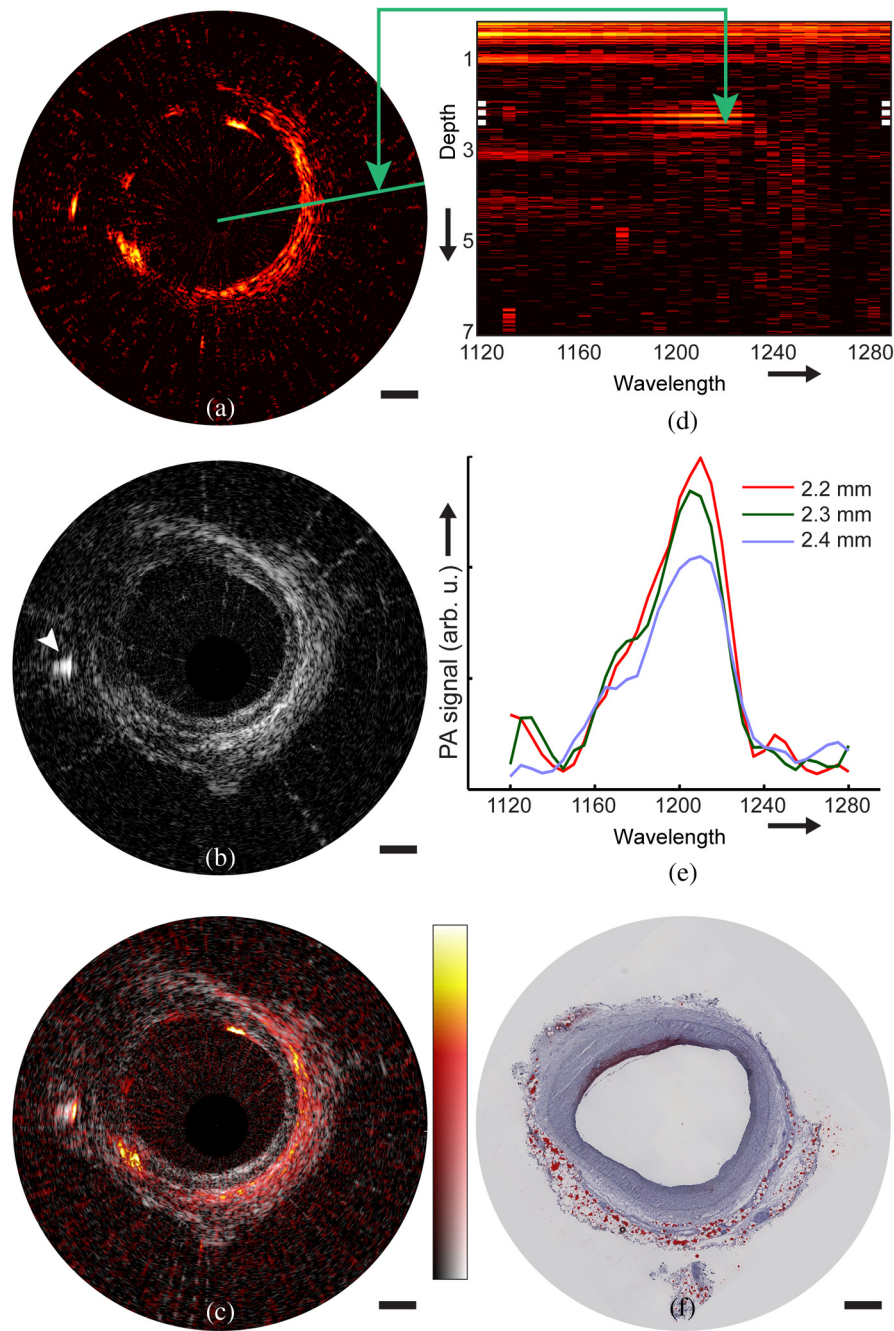
Fig. 2 Spectroscopic IVPA imaging. Coregistered IVPA and IVUS data are processed to create IVPA (a), IVUS (b) and combined IVPA/IVUS (c) images. At selected angular positions, indicated by the green line, 2D spectral IVPA (d) data are recorded by changing the wavelength of the light while keeping the catheter at rest. (e) Spectra at several locations in the vessel wall are extracted (f) IVPA and IVUS images are matched to histology stains for tissue characterization. Scale bars indicate 1 mm. Dynamic range for both ultrasound (grayscale) and Photoacoustic (PA, black-red-yellow) is 28 dB.

The magnitude of the locally generated PA signal is dependent on the local fluence, the absorption coefficient and the Grüneisen parameter of the tissue. The Grüneisen parameter, representing the thermo-acoustic efficiency, is dependent on the sound speed, the thermal expansion coefficient, and the specific heat at constant pressure. It therefore varies between different tissue types. Since the differences in local fluence are negligible within a small wavelength range, local variations in the PA signal amplitude with wavelength can be interpreted as changes in the absorption coefficient. We concentrated on the spectral range near 1200 nm where a prominent harmonic of the C—H stretch vibrational mode signals the presence of lipids.[28] Moreover, we take advantage of the fact that the absorption spectrum of connective tissue is markedly different from that of lipids in this wavelength range, while the absorption of water is relatively low. We analyzed the data and determined the 32 times averaged normalized PA spectra for the three lipids.

Robustness of the spectra was investigated by studying the individual variations in single-shot spectra, and monitoring the spectral shape for different depths in a sample. The stability of

the spectrum was evaluated by repeating the measurement several times over 75 min.

2.5 PA Spectroscopy of Human Coronary Arteries

At each imaging location, in addition to the IVPA/IVUS images acquired at several excitation wavelengths, full spectral scans were made at particular angular locations, which were selected based on IVUS morphology. Spectral PA data were recorded from 715 to 1800 nm with 5-nm steps. The data were then processed, as illustrated in Fig. 3. After the bandpass filtering operation described above, we selected regions containing the tissue and reference signals. The reference data contain nonsaturated signal close to the catheter that is due to light absorption in the catheter, which generates image artifacts. The amplitude of this signal was used to correct for variations in light intensity. Subsequently, the data were upsampled, jitter corrected, and downsampled to the original sample frequency. The data in the signal region was then Tukey windowed and corrected for variations in the light intensity using the jitter corrected reference data. We extracted the envelope of the tissue signal. Next, locations of high signal intensity were chosen automatically by selection of all peaks above a certain threshold in the 1195 nm enveloped signal trace. Spectra at those locations were noise filtered using a fourth order digital smoothing polynomial (Savitzky–Golay; SG) filter. Resulting spectra were compared to the PA spectra of cholesterol, cholesterol oleate, and cholesterol linoleate determined on the pure compounds, and to reference absorption spectra of collagen, elastin and a fatty acid mixture from literature.[29]

2.6 Histopathology of the Atherosclerotic Human Arteries

After imaging, the arterial specimens were cut at the imaging plane and serially sectioned for histology staining. The segment proximal from the image plane was fixed in 4%-buffered formaldehyde and embedded in paraffin. The tissue block was serially sectioned (5-μm thickness) at the imaging plane and stained by Hematoxylin–Eosin (H&E) and Resorcin–Fuchsin (RF). The segment distal from the imaging plane was embedded in optimal cutting temperature compound (Tissue-Tek®, Sakura Finetek Europe B.V.), frozen in isopentane vapor at 77 K, and stored at −80°C until serial sectioning (20-μm thickness) for Oil Red O (ORO) and H&E. Tissue sections were viewed and digitized using a whole-slide scanner (Nanozoomer, Hamamatsu Photonics, K.K., Hamamatsu City, Japan). The ORO staining identifies lipids (stained red). The H&E stained sections were used to assess tissue morphology.
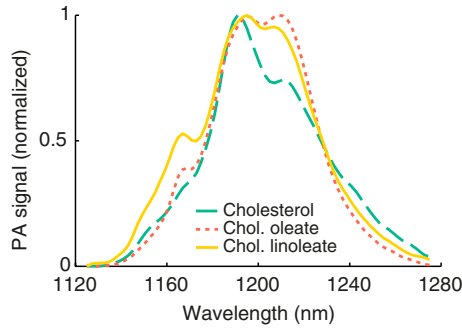
3 Results

3.1 PA Spectroscopy of Cholesterol and Cholesterol Derivates

Measurement of the PA signal of cholesterol, cholesterol oleate, and cholesterol linoleate in the 1200-nm range yielded three distinct PA spectra (Fig. 4). The absorption features in this wavelength range are caused by the second overtones of the vibrational modes of the C─H bonds in the molecules.[28,29] Wavelength shifts and intensity changes between the spectra of cholesterol, cholesterol oleate, and cholesterol linoleate originate from the differences in their molecular structures: the
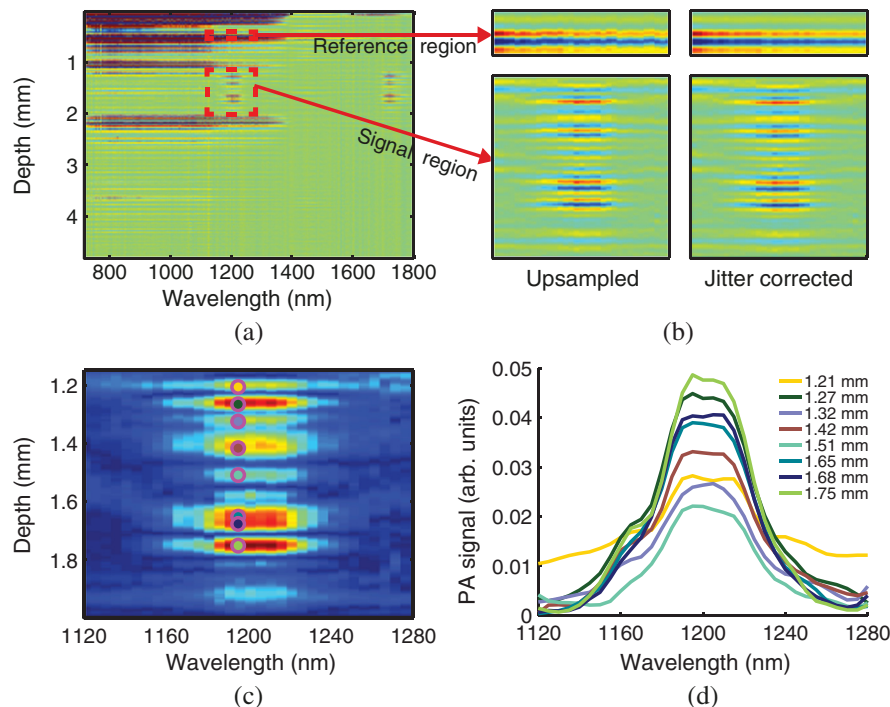
Fig. 3 Spectroscopic intravascular photoacoustics (sIVPA) data processing to obtain depth-resolved IVPA spectra. (a) Band pass filtered PA traces at different wavelengths. Regions containing the tissue (bottom rectangle) and reference (top rectangle) signals are indicated. (b) Upsampling and jitter correction. (c) Light intensity-corrected data in the tissue signal region with colored circles marking peaks above a certain threshold in the signal envelope of the PA trace at 1195 nm. (d) Resulting spectra at those sites after noise filtering.

Fig. 4 Absorption spectra of cholesterol, cholesterol oleate, and cholesterol linoleate in the 1200-nm wavelength region as recorded by PA spectroscopy exhibit clear differences.

cholesterol esters have a fatty acid tail that consists mainly of CH_2 groups. The two highest peaks at ~1196 (1192 nm for cholesterol) and 1210 nm are associated with the asymmetrical stretching modes of the methyl (CH_3) and methylene (CH_2) group vibrations, respectively, while the symmetrical stretching modes of the same groups are visible only as a shoulder or inflection points around 1151 and 1167 nm, respectively.

The robustness of the recorded spectra was evaluated by studying the reproducibility of spectra without averaging and by comparing averaged sets at different depths. Figure 5 summarizes the results of these experiments for one of the pure lipid compounds investigated. In Fig. 5(a), the difference between unaveraged spectra is shown to be very small, in the order of a few percent of the total signal. We attribute the remaining variation to measurement noise that is not adequately smoothed

by the SG filter. Likewise, the spectra acquired at different depths are very similar [Fig. 5(b)].

The stability of the absorption spectrum over time is demonstrated by the data in Figs. 5(c) and 5(d): we see a moderate increase in signal strength, but no change in spectral shape. The change in signal amplitude may be attributed to variations in packing density and water content in the lipid sample. Over time, the (unsaturated) lipid in the container is likely to be oxidized. We see that the spectrum appears to be robust against such variations.

## 3.2 IVPA Spectroscopy of Human Coronary Arteries

Dual-modality imaging of a human coronary atherosclerotic artery (left anterior descending artery, male aged 56) *ex vivo* revealed a large eccentric plaque with high PA signal intensities [Fig. 6(a)] in the regions that were shown to be lipid-rich by histology [Fig. 6(b)]. The artery was embedded in peri-adventitial fat. An elaborate discussion of the separate IVUS and IVPA images at 1210 and 1230 nm may be found in Ref. 21.

Positive confirmation of the presence and identification of lipids requires wavelength-dependent measurement. In the two directions indicated by the white lines, labeled as # and *, in the IVPA/IVUS image, we acquired spectroscopic IVPA data. Spectra in tissue were composed from one single IVPA acquisition per wavelength, creating a data set as in Fig. 2(d), and then plotting the signal strength as a function of wavelength at a single pixel in depth. We show the IVPA spectra of different tissues in Fig. 6.

The direction marked as # contained atherosclerotic plaque [Fig. 6(c)], while the line-of-sight marked as * intersected with the lipid-rich diseased intima [Fig. 6(d)], the adventitia
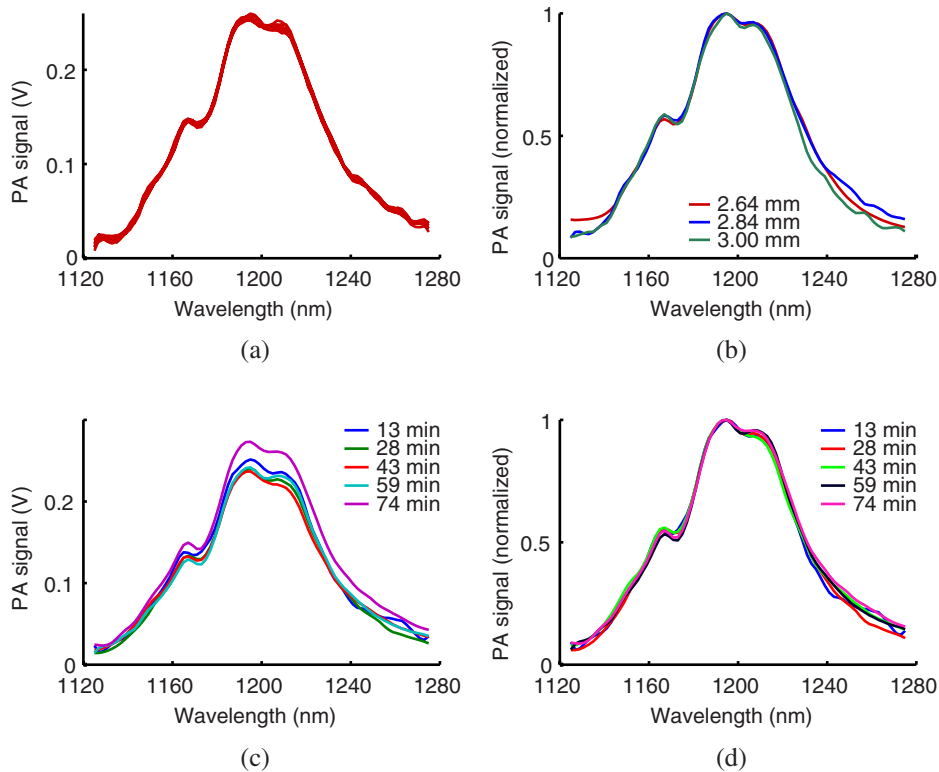
Fig. 5 Robustness of lipid PA spectroscopy showing data from cholesterol linoleate as an example. (a) Comparison of "single-shot" spectra. (b) Spectra obtained at different depths. (c) Evolution of the spectral amplitude over time. (d) Data from panel (c) after normalization.
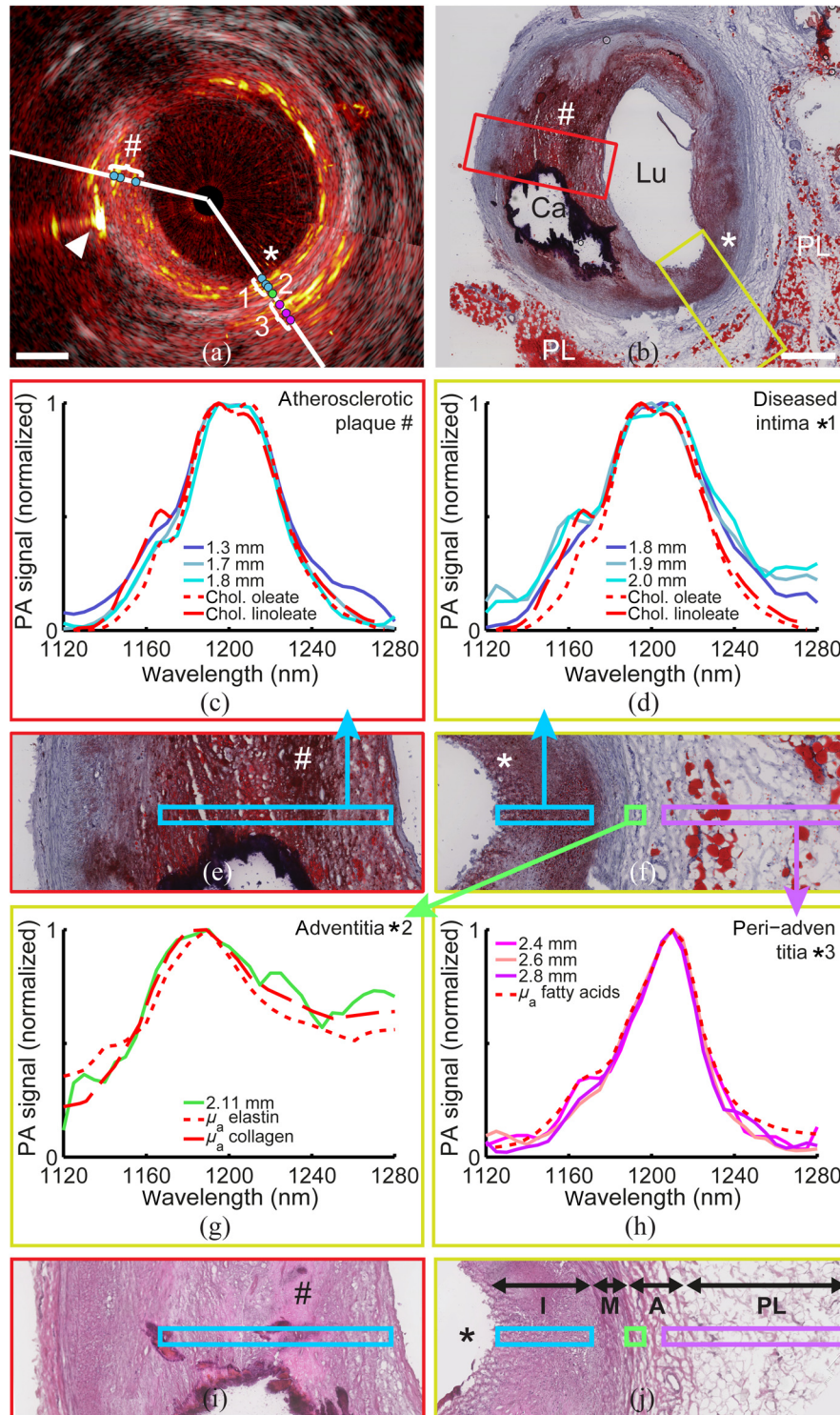
Fig. 6 IVPA spectra of a human atherosclerotic coronary artery, *ex vivo*. (a) Dual-modality IVPA/IVUS image, arrowhead indicates suture needle. Along the white lines (# and *), spectral IVPA data were obtained. Normalized IVPA spectra at the locations of the dots are shown in (c) (#, blue dots), (d) (*, blue dots), (g) (*, green dot), and (h) (*, purple dots), compared to absorption spectra obtained in Fig. 4 and reference spectra for collagen, elastin, and fatty acids from literature.[29] (b) Histology section of the site imaged in (a), showing near circumferential intimal lipid accumulation (red) and presence of a calcification (Ca). The lipid rich core (#) and pathological intimal thickening (PIT; *) are magnified (3×) in (e) and (f), respectively, showing the locations where the IVPA spectral data are recorded. (i) Hematoxylin–Eosin (H&E) histologic stain of the area #, showing reduced cellularity in the plaque. (j) H&E stain of the area *, showing PIT and an intact media. Spectra locations in (c), (d), (g), and (h) are stated in millimeter from the catheter tip. Oil Red O stain, Lu = lumen, PL = peri-adventitial lipid. Scale bars indicate 1 mm. Dynamic range of IVPA and IVUS image is 40 dB; color scales as in Fig. 2.

[Fig. 6(g)]—the outermost layer of the vessel wall consisting of connective tissue—and a region of peri-adventitial tissue [Fig. 6(h)] composed mainly of adipocytes (fat cells) containing fatty acids.[29]

We found that the lipid laden atherosclerotic plaque and diseased intima [Figs. 6(c) and 6(d), respectively] both had IVPA spectra that closely resemble the reference PA spectra of cholesterol oleate and cholesterol linoleate obtained on the pure compounds. This finding was in agreement with the assessment of the corresponding areas in the histological sections [Figs. 6(e), 6(i), 6(f), and 6(j), respectively], that showed lipid-rich foam cells and extracellular lipid droplets, but no cholesterol crystals. The H&E stain [Figs. 6(i) and 6(j)] shows differences in cell density and orientation of cells in the intima (cell nuclei are colored blue/purple). The lower cell density of the more central plaque areas [Fig. 6(i)] indicates a more advanced state of atherosclerosis with extracellular lipids (larger red spots in central region of ORO stain [Fig. 6(e)]. H&E [Fig. 6(j)] also illustrates the much larger adipocytes in the peri-adventitial region. The IVPA spectrum found in the adventitia, shown in Fig. 6(g), was very similar to both the absorption spectra of elastin and collagen, while the IVPA spectra of the lipid-rich peri-adventitial tissue [Fig. 6(h)] resembled the absorption spectrum of the reference fatty acid mixture.[29]

4 Discussion

PA imaging adds highly detailed chemical information to existing diagnostic techniques for coronary atherosclerosis. We show its ability to outline fat deposits and to distinguish between plaque lipids and peri-adventitial lipids. The composition of lipid-rich plaques can be differentiated in cholesterol and a range of cholesterol esters by PA spectroscopy, opening up a new dimension for *in vivo* plaque characterization. Characteristic spectral signatures of collagen and elastin identify the adventitia; a contrast that may be of use in plaque imaging as well. No other clinically feasible imaging technique images the vessel wall and atherosclerotic plaque composition with such chemical specificity.

IVPA is unique in its ability to distinguish the lipids present in atherosclerotic plaque at a high resolution of ∼100 μm. Its visualization of different constituents of atherosclerotic plaques and deeper layers of the vessel wall is based on the intrinsic contrast in optical absorption between tissue types. The optical absorption spectrum is a much more specific tissue identification criterion than parameters like the attenuation and backscatter coefficients, which other techniques rely on for plaque composition. The background for this difference is that both optical scattering (which dominates optical attenuation) and acoustic absorption (which dominates acoustic attenuation) are slowly varying with frequency, so distinctive features like those seen in Fig. 2 are not available for detailed composition imaging. NIRS, like IVPA, uses absorption spectra to determine lipid content, but does not have depth-resolving capability. As a consequence, it can identify the presence but not the amount or the position of the lipid accumulation. NIRS has been combined with IVUS to add structural information but exact localization of the lipid core cannot be realized.[11]

With the composition information provided by IVPA, tissue maps can be created, showing the location of different kinds of lipids (free cholesterol, cholesterol esters in foam cells or extracellular lipid droplets) as well as other tissue types (collagen, elastin) on top of the morphological picture provided by IVUS.

Cholesterol oleate and cholesterol linoleate together account for more than 67% of cholesterol esters present in lipid-rich lesions, while cholesterol esters and cholesterol together make up 79% of total lipids.[30] In the present study, we investigated the contribution of the three most significant components in the plaque lipid spectrum. Further studies need to establish the level of detail to which IVPA can unravel the lipid composition of plaques; this is both a fundamental question of the chemical specificity of the different absorption spectra as well as a technical question: how accurately can we measure the spectra to exploit that specificity, at a practical number of wavelengths? It is unknown at present how much composition detail is needed to establish whether a lesion is progressing toward rupture, quiescent, or regressing toward stability. Such data could be derived from future clinical imaging trials, which will determine the value of sIVPA cholesterol subtyping for vulnerable plaque risk prediction. A possible first step in this direction is a sIVPA study to show the difference in spectra between fatty streaks, necrotic cores, and fibrotic plaques. Beyond lipid composition, IVPA may be able to distinguish other tissue types or plaque characteristics that play a role in coronary artery disease, such as calcium, macrophages, and intraplaque hemorrhage by choosing a different wavelength range or using exogenous contrast. Spectral unmixing techniques,[31] or optimal wavelength selection schemes,[32] are expected to become useful tools in the development of sIVPA for imaging different plaque constituents.

Two issues that come into play when imaging *ex vivo* and need addressing are lipid oxidation and temperature. Unsaturated lipids, such as cholesterol oleate and cholesterol linoleate, become oxidized when imaged *ex vivo*. But lipids in atherosclerotic lesions are partially oxidized as well: in freshly obtained carotid and femoral atherosclerotic plaque ∼30% of plaque cholesterol linoleate was found to be oxidized, with CE18:2─OH and CE18:2═O (two oxidized forms of cholesterol linoleate) being the predominant forms.[33] However, since the number of C─H bonds does not change with oxidation, no change in the relative peak strengths in the absorption spectrum is expected; this supposition is strengthened by the results of the separate lipid PA measurements, where an increase in the level of oxidation of the lipids with time was anticipated, and the spectra remained structurally unchanged over time, as demonstrated in Fig. 5. Similarly, a change in temperature from body temperature to room temperature is not expected to influence the position of peaks or relative peak height within the IVPA spectra, since these are dependent on the molecular structure, which does not change with temperature. NIRS was validated under the same assumptions[10] and spectra were shown to be similar *ex vivo* and *in vivo*.[34]

For translation to *in vivo* imaging, several changes to the system need to be realized. The catheter needs to be further miniaturized and fitted with a compatible outer sheath. It needs to be coupled to a real-time imaging system through an interface unit containing a motorized fiber optical and pullback system, to make continuous rotation and simultaneous translation possible. Furthermore, the minimum number of wavelengths required to determine tissue type needs to be established, reducing acquisition time. A sufficient level of tissue composition information may be obtained by using three wavelengths only, if chosen wisely. Single-wavelength lasers that can be combined to design a system, which generates such wavelengths at fast enough pulse rates to achieve clinically feasible frame rates are currently under development.[35]

We demonstrated the ability of IVPA to distinguish lipid types as well as other kinds of tissues in coronary atherosclerosis. This functionality can aid in gaining further understanding of the disease: it adds a new dimension to *in vivo* studies of progression and regression processes of plaque. This new functionality has a direct application in more complete visualization of coronary wall pathology for clinical decision making. Impacts in the medium to longer term include the introduction of highly detailed chemical imaging biomarkers as an endpoint in studies evaluating pharmacological therapies, and to measure the response of the arterial system to lifestyle changes in clinical trials. Imaging lipid composition in atherosclerotic plaque *in vivo*, and relating that information to its stage of advancement will contribute to further understanding of the development of the natural history of atherosclerosis. Finally, detailed imaging of plaque biochemistry and lipidomics may provide a jump-off point for personalized medicine in interventional cardiology, if we can predict the vascular response to an intervention of a specific site in a specific artery in a specific patient.

References

1. *Global Atlas on Cardiovascular Disease Prevention and Control*, World Health Organization, Geneva (2011).
2. E. Falk, P. K. Shah, and V. Fuster, "Coronary plaque disruption," *Circulation* **92**(3), 657–671 (1995).
3. J. A. Schaar et al., "Terminology for high-risk and vulnerable coronary artery plaques," *Eur. Heart J.* **25**(12), 1077–1082 (2004).
4. R. Virmani et al., "Lessons from sudden coronary death: a comprehensive morphological classification scheme for atherosclerotic lesions," *Arterioscler. Thromb. Vasc. Biol.* **20**(5), 1262–1275 (2000).
5. R. D. Madder et al., "Features of disrupted plaques by coronary CT Angiography: correlates with invasively-proven complex lesions," *Circ. Cardiovasc. Imaging* **4**(2), 105–113 (2011).
6. R. Virmani et al., "Pathology of the vulnerable plaque," *J. Am. Coll. Cardiol.* **47**(Suppl. 8), C13–C18 (2006).
7. D. M. Small, "George Lyman Duff memorial lecture. Progression and regression of atherosclerotic lesions. Insights from lipid physical biochemistry," *Arterioscler. Thromb. Vasc. Biol.* **8**(2), 103–129 (1988).
8. C. V. Felton et al., "Relation of plaque lipid composition and morphology to the stability of human aortic plaques," *Arterioscler. Thromb. Vasc. Biol.* **17**(7), 1337–1345 (1997).
9. M. Puato et al., "Atorvastatin reduces macrophage accumulation in atherosclerotic plaques: a comparison of a nonstatin-based regimen in patients undergoing carotid endarterectomy," *Stroke* **41**(6), 1163–1168 (2010).
10. C. M. Gardner et al., "Detection of lipid core coronary plaques in autopsy specimens with a novel catheter-based near-infrared spectroscopy system," *JACC Cardiovasc Imaging* **1**(5), 638–648 (2008).
11. S. Garg et al., "First use in patients of a combined near infra-red spectroscopy and intra-vascular ultrasound catheter to identify composition and structure of coronary plaque," *EuroIntervention* **5**(6), 755–756 (2010).
12. S. Achenbach et al., "Detection of calcified and noncalcified coronary atherosclerotic plaque by contrast-enhanced, submillimeter multidetector spiral computed tomography: a segment-based comparison with intravascular ultrasound," *Circulation* **109**(1), 14–17 (2004).
13. P. W. Serruys et al., "Effects of the direct lipoprotein-associated phospholipase A(2) inhibitor darapladib on human coronary atherosclerotic plaque," *Circulation* **118**(11), 1172–1182 (2008).
14. T. Nozue et al., "Statin treatment for coronary artery plaque composition based on intravascular ultrasound radiofrequency data analysis," *Am. Heart J.* **163**(2), 191–199 (2012).
15. P. Libby and W. Sasiela, "Plaque stabilization: can we turn theory into evidence?" *Am. J. Cardiol.* **98**(11A), 26P–33P (2006).
16. L. W. Klein, "Atherosclerosis regression, vascular remodeling, and plaque stabilization," *J. Am. Coll. Cardiol.* **49**(2), 271–273 (2007).
17. P. Beard, "Biomedical photoacoustic imaging," *Interface Focus* **1**(4), 602–631 (2011).
18. H. Crazzolara et al., "Analysis of the acoustic response of vascular tissue irradiated by an ultraviolet-laser pulse," *J. Appl. Phys.* **70**(3), 1847–1849 (1991).
19. R. K. Al Dhahir, P. E. Dyer, and Z. Zhu, "Photoacoustic studies and selective ablation of vascular tissue using a pulsed dye laser," *Appl. Phys. B* **51**(1), 81–85 (1990).
20. P. C. Beard and T. N. Mills, "Characterization of post mortem arterial tissue using time-resolved photoacoustic spectroscopy at 436, 461 and 532 nm," *Phys. Med. Biol.* **42**(1), 177–198 (1997).
21. K. Jansen et al., "Intravascular photoacoustic imaging of human coronary atherosclerosis," *Opt. Lett.* **36**(5), 597–599 (2011).
22. B. Wang et al., "Detection of lipid in atherosclerotic vessels using ultrasound-guided spectroscopic intravascular photoacoustic imaging," *Opt. Express* **18**(5), 4889–4897 (2010).
23. T. J. Allen et al., "Spectroscopic photoacoustic imaging of lipid-rich plaques in the human aorta in the 740 to 1400 nm wavelength range," *J. Biomed. Opt.* **17**(6), 061209 (2012).
24. B. Wang et al., "Plasmonic intravascular photoacoustic imaging for detection of macrophages in atherosclerotic plaques," *Nano Lett.* **9**(6), 2212–2217 (2009).
25. C. Stegemann et al., "Comparative lipidomics profiling of human atherosclerotic plaques / clinical perspective," *Circ.: Cardiovasc. Genet.* **4**(3), 232–242 (2011).
26. K. Jansen et al., "An intravascular photoacoustic imaging catheter," in *2010 IEEE Ultrasonics Symposium (IUS)*, pp. 378–381 (2010).
27. Q. Zhou et al., "PMN-PT single crystal, high-frequency ultrasonic needle transducers for pulsed-wave Doppler application," *IEEE Trans. Ultrason. Ferroelectr. Freq. Control* **54**(3), 668–675 (2007).
28. R. T. Holman and P. R. Edmondson, "Near-infrared spectra of fatty acids and some related substances," *Anal. Chem.* **28**(10), 1533–1538 (1956).
29. C. L. Tsai, J. C. Chen, and W. J. Wang, "Near-infrared absorption property of biological soft tissue constituents," *J. Med. Biol. Eng.* **21**(1), 7–14 (2001).
30. S. S. Katz, G. G. Shipley, and D. M. Small, "Physical chemistry of the lipids of human atherosclerotic lesions. Demonstration of a lesion intermediate between fatty streaks and advanced plaques," *J. Clin. Invest.* **58**(1), 200–211 (1976).
31. P. Wang et al., "Mapping lipid and collagen by multispectral photoacoustic imaging of chemical bond vibration," *J. Biomed. Opt.* **17**(9), 096010 (2012).
32. G. P. Luke, S. Y. Nam, and S. Y. Emelianov, "Optical wavelength selection for improved spectroscopic photoacoustic imaging," *Photoacoustics* **1**(2), 36–42 (2013).
33. C. Suarna et al., "Human atherosclerotic plaque contains both oxidized lipids and relatively large amounts of a-tocopherol and ascorbate," *Arterioscler. Thromb. Vasc. Biol.* **15**(10), 1616–1624 (1995).
34. S. Waxman et al., "In vivo validation of a catheter-based near-infrared spectroscopy system for detection of lipid core coronary plaques initial results of the SPECTACL study," *JACC Cardiovasc. Imaging* **2**(7), 858–868 (2009).
35. R. Li et al., "Compact high power barium nitrite crystal-based Raman laser at 1197 nm for photoacoustic imaging of fat," *J. Biomed. Opt.* **18**(4), 040502 (2013).

Biographies of the authors are not available.